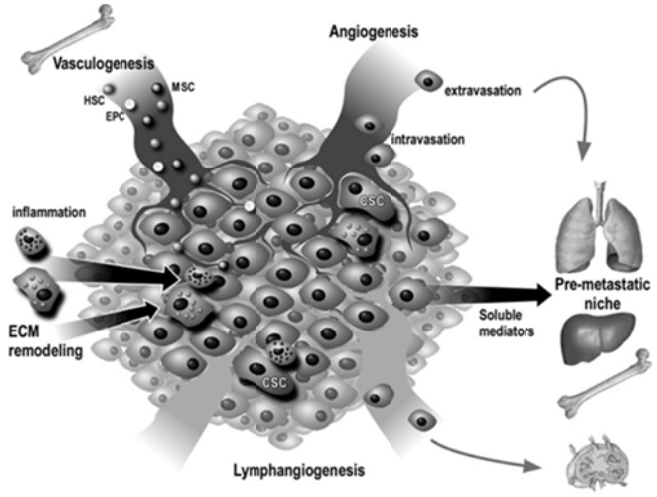

Figure 1: Metastatic dissemination and tumour microenvironment. In addition to the sprouting of neighbouring pre-existing vessels, tumoural angiogenesis is supported by the mobilization of different cell types including hematopoietic stem cells (HSC), endothelial progenitor cells (EPC) and mesenchymal stem cells (MSC). Lymphangiogenesis facilitates metastasis by providing an alternative route of dissemination. Primary tumoural cells could induce the establishment of a pre-metastatic niche preceding metastatic colonization of the targeted organ. CSC = cancer stem cells

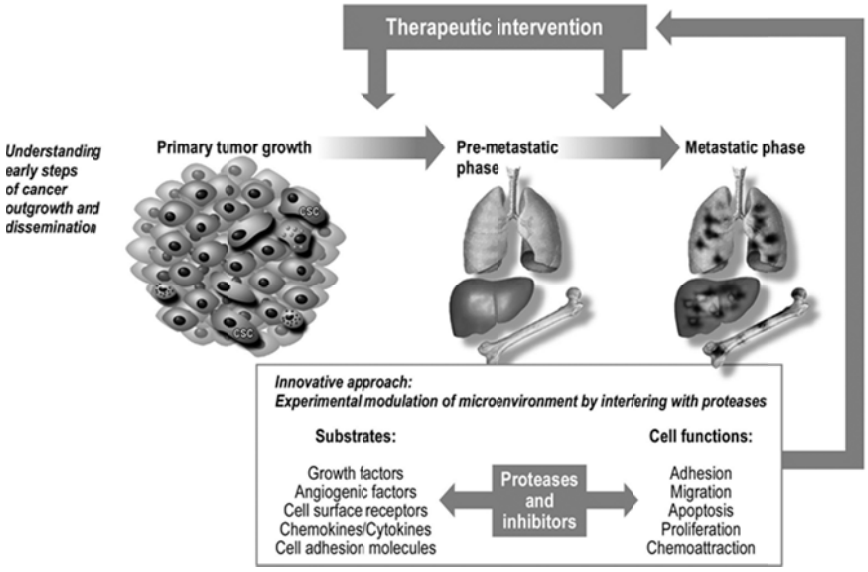

Figure 2: Aims and approaches used by the *MEM consortium*. The study provides new insights into the interplay between cancer cells, cancer stem cells (CSC) and their microenvironment, both at primary and secondary sites. Modulation of tumour microenvironment has been achieved by interfering with proteases that are central mediators of a complex molecular network, as well as key regulators of various cell functions.

Modification of the protease Web on:	Tumor-promoting effects ➔Increased tumor growth, angiogenesis and/or tumor cell invasion	Anti-tumor effects ➔ Reduced tumor growth, angiogenesis and/or Tumor cell invasion
1. The tumor Compartment	Overexpression of ADAMTS-1 MT1-MMP (MMP14) MT4-MMP (MMP-17)	Overexpression of ADAMTS-12 ADAMTS-12 MMP8
2. The host Compartment	Gene deficiency of MMP8 MMP19 ADAMTS-12	Gene deficiency of PAI-1 Stefin-B

Table 1: summary of the tumour-promoting effects and the anti-tumoural actions of proteases and their inhibitors demonstrated by the MEM consortium.

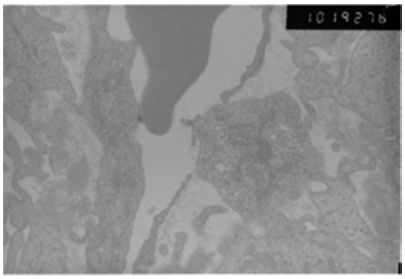

Figure 3: Illustration of the intravasation of a tumour cell frequently observed in MT4-MMP overexpresssing tumours, but not in control tumours.

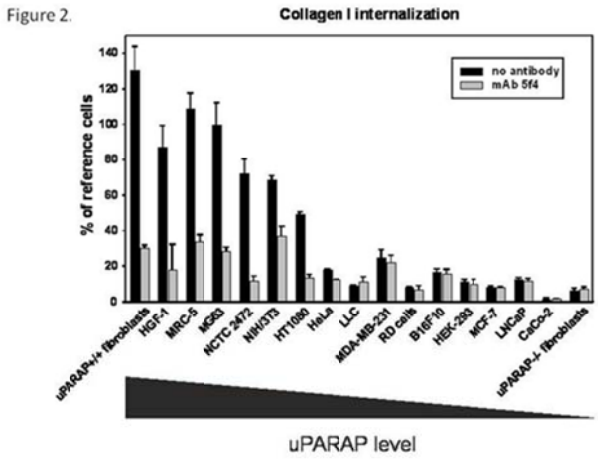

Figure 4: uPARAP/Endo180 mediates collagen internalization in a variety of cell types. Collagen internalization is inhibited by mAb 5f4 for a variety of established cell lines. Collagen internalization was measured for each cell line. Internalization was carried out in the absence of antibody (black columns) or in the presence of 10 µg/ml of mAb 5f4 (grey columns). The cell lines are ranked in the diagram according to their level of uPARAP/Endo180 expression, with the highest expressing cells to the left.

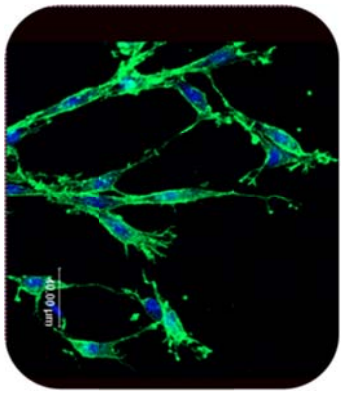

Figure 5: Illustration of lymphatic endothelial cells spreading from a lymphatic vessel fragment. Endothelial cells are labeled in green (with an anti-LYVE-1 antibody) and nuclei are stained in blue. This model reproduces the different steps of the lymphangiogenic process observed during cancer progression, both at primary site and secondary sites of tumour growth.

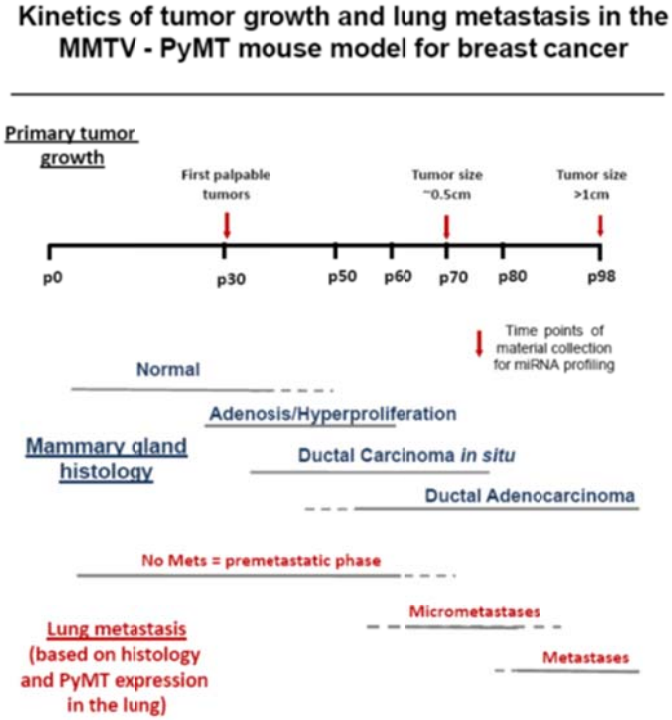

Figure 6: Kinetics of tumor growth and metastasis formation.

Table 2

Table 1 Tumor-associated immune cells

Cell type	*Marker*	*PymT$^{+/0}$;wt* *% of total ± s.e.m.*	*PymT$^{+/0}$;Tg(CTSB)$^{+/0}$* *% of total ± s.e.m.*	
CD4 + T cells	CD4	0.60 ± 0.17	0.61 ± 0.23	NS
CD8 + T cells	CD8	1.05 ± 0.15	1.79 ± 0.47	NS
B cells	CD19	0.51 ± 0.07	1.47 ± 0.55	$P<0.05$
Macrophages	F4/80	2.00 ± 0.30	2.83 ± 0.66	NS
Neutrophils	7/4 Antigen[a]	1.77 ± 0.41	2.25 ± 0.75	NS
Mast cells	CAE	18.8 ± 3.1[b]	31.7 ± 1.5[b]	$P<0.01$

Quantification of distinct immune cell types, including T and B cells, macrophages and neutrophils as percentage of total cells by flow cytometry ($n = 8$–12 per genotype). Mast cells were identified by CAE histochemistry and the number of CAE + cells per mm^2 of tumor stroma was calculated from three independent sectional planes ($n = 4$ per group). Data are presented as means and standard errors; statistical analysis was done by Student's *t*-test.
[a]Detected by anti-mouse neutrophils/Clone 7/4; rat IgG2a (Cedarlane, Burlington, Ontario, Canada).
[b]Number of mast cells per mm^2 tumor stroma.

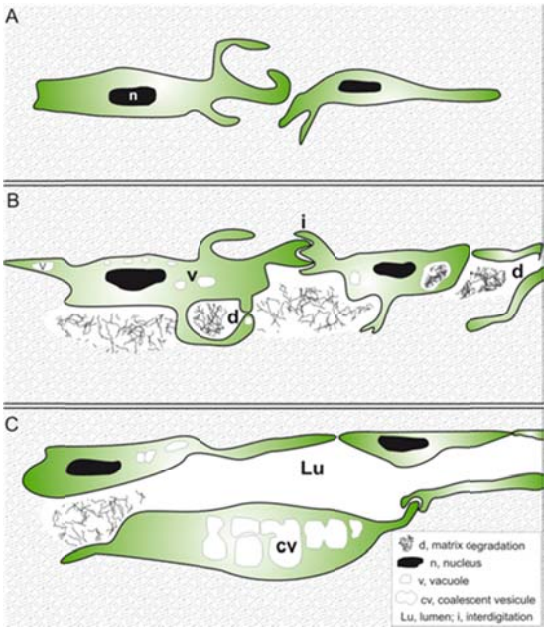

Figure 7: Model of formation of new lymphatic vessels during the process of lymphangiogenesis (see description in the text).

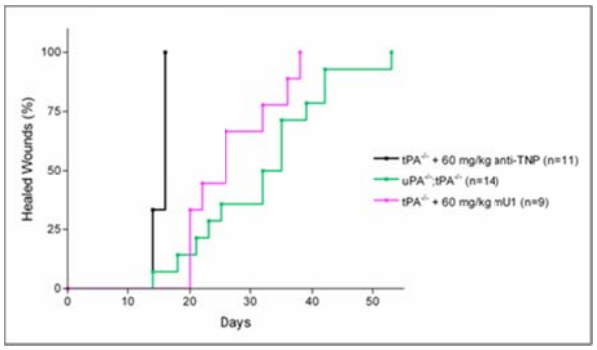

Figure 8: mU1 retards wound healing, demonstrating the efficient blocking of uPA function in a physiological invasive process *in vivo*.

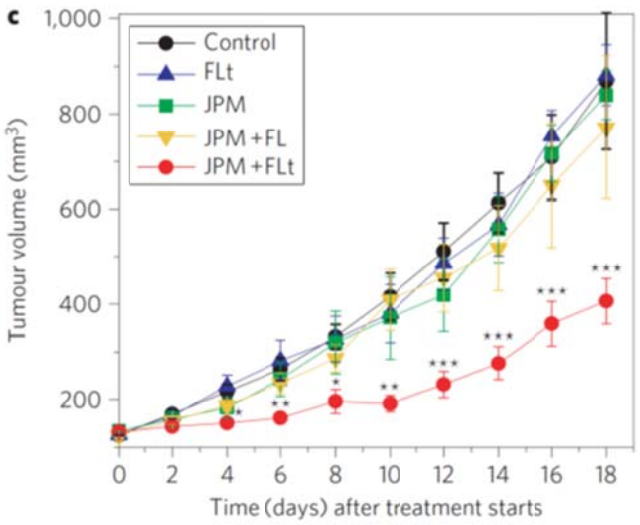

Figure 9: Anti-tumour effect of magnetically targeted ferri-liposomes containing JPM-565. Tumour volumes for each treatment day for the different treatment groups. Mice were treated with ferri-liposomes without (FL) and with magnetic targeting (FLt), and JPM-565 (JPM) combinations as represented by the '+' sign.